SPACE-TIME DISCONTINUOUS GALERKIN METHOD FOR WET-CHEMICAL ETCHING OF MICROSTRUCTURES

J.J. Sudirham, R.M.J. van Damme and J.J.W. van der Vegt

University of Twente, Department of Applied Mathematics
P.O. Box 217, 7500 AE Enschede, The Netherlands
e-mail: j.j.sudirham@math.utwente.nl, r.m.j.vandamme@math.utwente.nl,
j.j.w.vandervegt@math.utwente.nl

Key words: wet-chemical etching, discontinuous Galerkin finite element methods

Abstract. *In this paper we discuss the application of a space-time discontinuous Galerkin finite element method for convection-diffusion problems to the simulation of wet-chemical etching of microstructures. In the space-time DG method no distinction is made in the discretization between the space and time variables and discontinuous basis functions are used both in space and time. This approach results in an efficient numerical technique to deal with time-dependent flow domains as occur in wet-chemical etching, while maintaining a fully conservative discretization. The method offers great flexibility in mesh adaptation and special attention is given to the generation of an initial solution and mesh when there is no etching cavity yet. Numerical simulations of the etching of a two-dimensional slit are discussed for different regimes, namely diffusion-controlled and convection-dominated etching. These results show good agreement with analytical results in the diffusion-controlled regime. Using a simple model for the fluid velocity the typical asymmetric etching cavities are obtained in the convection dominated regime and the results agree qualitatively well with those obtained from full Navier-Stokes simulations.*

1

1 INTRODUCTION

Etching is a production technique which is widely used in high-technology. Examples are the fabrication of semi-conductors, microsystems and transducers. Etching is also important for the mass production of complicated objects with small features, such as the production of shadow masks in color TV's and printed circuit boards in electronics. In all these cases one uses a key benefit of etching, namely that the process is independent of the complexity of the design. This makes etching ideally suited for the production of complicated small objects. In this paper we focus on wet-chemical etching, which is an important etching technique and widely used for the etching of thin films. In wet-chemical etching an acid fluid is used to dissolve the material which is not protected by a mask. This results in an effective etching technique, but one has to deal with several inaccuracies, for instance under-etching near the mask edge, in particular near sharp corners, and the interaction between nearby cavities. There is, therefore, a need to better understand and control the different phenomena in wet-chemical etching.

Mathematical models based on the fundamental principles of transport and reaction phenomena are useful in predicting the shape of the object produced by the etching process and provide insight into the important mechanisms. This can be done using analytical techniques after some simplifying assumptions are made [4, 5], and also provides simple design rules. For more complicated structures and systems numerical simulations are more useful, but the simulation of wet-chemical etching is a non-trivial task. The numerical method should be able to analyze the fluid flow and transport phenomena in complex deforming geometries. In particular one has to deal with free boundaries, thin boundary layers near the etching surface, and singularities near sharp corners, such as the mask edge. Unstructured hp-discontinuous Galerkin (DG) finite element methods, delivering high-order accuracy and the flexibility to deal with complex deforming geometries, satisfy these requirements. In this paper we will apply a new space-time discontinuous Galerkin finite element method for convection-diffusion problems, which we derived in [8, 9], to the simulation of the etching of small structures.

The space-time DG method has as key feature that time is treated as an extra dimension which makes the method particularly useful for problems with time-dependent flow domains. Since the main features of the space-time DG method are discussed and analyzed in detail in [8, 9] (see also [1, 2]), we will focus in this paper on the application of this technique to etching, which is demonstrated with the etching of a slit. Special attention will be given to problems caused by the moving and deforming flow domain boundaries and the computation of the initial solution.

The organization of this paper is as follows. In Section 2 we state the physical problem and give the equations that govern the transport problems in wet-chemical etching and the movement of the cavity boundary. In Section 3 we discuss the geometry of the space-time domain and we briefly summarize the space-time DG formulation for the convection-diffusion equation and the moving boundary equation in Section 4. The technique to

2

adapt the computational mesh is discussed in Section 5. We also discuss the benefits of our new mesh adaptation approach compared to other techniques for similar applications. Finally, in Section 6 we discuss numerical results for the etching of a slit. We consider two cases, where the etching process is either diffusion-controlled or a convection-dominated. Some concluding remarks are made in Section 7.

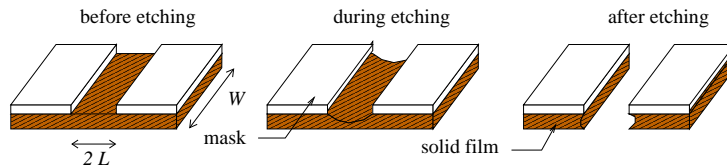## 2   THE PHYSICAL PROBLEM AND TRANSPORT EQUATIONS

Figure 1: Illustration of etching process.

An illustration of the etching process under consideration is shown in Fig. 1. Assuming that the length W is large compared to the half width of the cavity L, we can consider the etching process of a slit to be a two-space dimensional problem, as we will do in this paper, see Fig. 2.
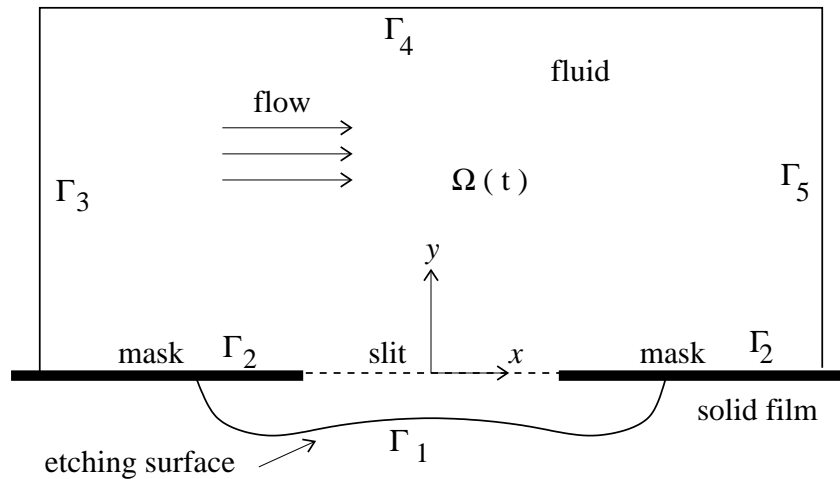
Figure 2: Flow domain of a slit.

A solid film, partially protected by a mask, is placed in an acid fluid which flows past the film. The acid fluid contains an etchant which reacts with the film, but is inert against the mask. Here we assume that only one species in the fluid is important in the etching process. The etchant is transported by convection and diffusion to the film surface where

it reacts, thereby dissolving the unprotected part of the film. As etching proceeds, the shape of the cavity evolves with time according to the etch rate distribution along the cavity, which depends on the concentration of the etchant inside the flow domain.

We introduce the following characteristic quantities: the length scale L, concentration scale c_i (inflow etchant concentration), and time scale L^2/D, with D the diffusion coefficient. The transport of the concentration c of the etchant in scaled variables is assumed to be governed by a convection-diffusion equation

$$\frac{\partial c}{\partial t} + u \cdot \nabla c - \nabla^2 c = 0, \quad \text{in } \Omega(t) \times (0, T), \tag{1}$$

where we assume that u is a prescribed velocity field. The value of velocity u is related to the Péclet number P_e, which is defined as

$$P_e = \frac{u_c L}{D},$$

with u_c a characteristic fluid velocity, e.g. the maximum of $|u|$ in the domain $\Omega(t)$. The magnitude of the Péclet number controls the type of process: for small values of P_e the process is diffusion-controlled, for large P_e the process is convection-dominated. The variable T is the final time of the process. The flow domain is bounded by the moving boundary Γ_1, the mask Γ_2, and the far field boundaries $\Gamma_3, \Gamma_4, \Gamma_5$. The above equation is accompanied by the initial condition $c = c_0$ and suitable boundary conditions at Γ_D and Γ_M, related to Dirichlet and mixed boundary conditions, respectively. At these boundaries, we define the following conditions

$$c = g_D \text{ on } \Gamma_D, \quad \text{and} \quad \nabla c \cdot \bar{n} + \alpha c = g_M \text{ on } \Gamma_M, \tag{2}$$

where g_D, g_M are given functions and $\bar{n}$ is the outward normal vector to $\Omega(t)$. The parameter α is a non-negative number and the value of this parameter at each boundary depends on the physics. For example for an outflow boundary we have $\alpha = 0$, whereas at the etching surface (Γ_1) it is related to speed of the dissolution process of the solid, and is referred to as the Sherwood number S_h, which is defined as

$$S_h = \frac{k\,L}{D},$$

where k is the reaction constant of dissolution process. For small values of S_h the process at the boundary is kinetically-controlled, for large S_h the process is reaction-controlled. In this paper, we will consider different magnitudes of S_h.

Whether the condition on each boundary Γ_i, $i \in \{1, \ldots, 5\}$ is Dirichlet or mixed, depends on the application. We give more details on these conditions for each application separately in Sec. 6. The velocity v of the moving cavity boundary Γ_1 in the direction of the outward normal is described by

$$v_n = -\beta^{-1} \nabla c \cdot \bar{n}, \tag{3}$$

with β a dimensionless material constant. Values of β for different materials can be found, e.g. in [5].

3 GEOMETRY OF THE SPACE-TIME DOMAIN

We consider a computational domain directly in space and time, denoted as $E \subset \mathbb{R}^3$. Let us consider the time interval $\mathcal{I} = (0, T)$, partitioned by an ordered series of time levels $0 = t_0 < t_1 < \ldots < t_{N_t} = T$. Denoting the nth time interval $I_n = (t_n, t_{n+1})$, we have $\mathcal{I} = \cup_{n=0}^{N_t-1} I_n$. The domain E is divided into N_t space-time slabs $E^n = E \cap I_n$ (Fig. 3a). Each space-time slab E^n is bounded by Ω_n, Ω_{n+1}, and $\mathcal{Q}^n = \partial E^n \setminus (\Omega_n \cup \Omega_{n+1})$, where Ω_n and Ω_{n+1} are the approximations to the domain $\Omega(t)$ at time t_n and t_{n+1}, respectively.
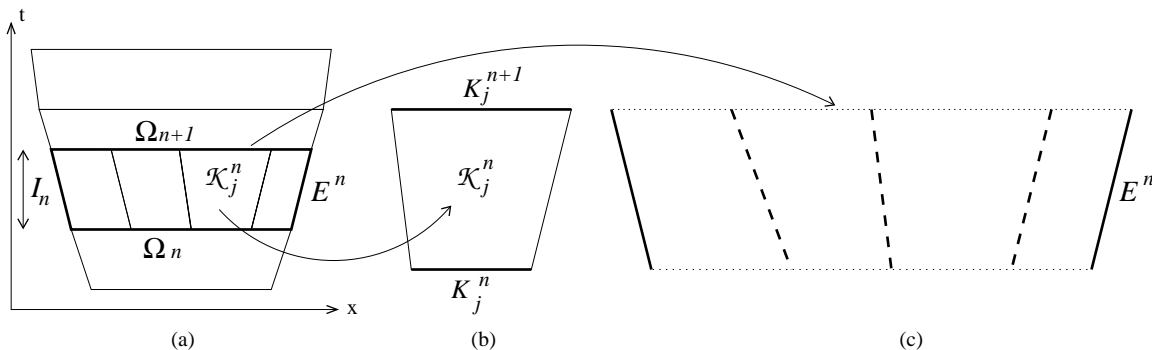

Figure 3: Illustration of the space-time domain for one space dimension. (a) Space-time domain. (b) Space-time element. (c) Sets of faces. Internal faces $\mathcal{S}_I^n$ (dashed line) and boundary faces $\mathcal{S}_B^n$ (solid line).

For the nth space time slab E^n, let the domains Ω_n and Ω_{n+1} be subdivided into N_n spatial elements $K_j^n = K_j(t_n)$ and $K_j^{n+1} = K_j(t_{n+1})$, respectively. Each space-time element $\mathcal{K}_j^n$ is then obtained by connecting K_j^n and K_j^{n+1} using linear interpolation in time (Fig. 3b). The element boundary $\partial \mathcal{K}_j^n$ is defined as a union of $K_j(t_n^+) = \lim_{\epsilon \downarrow 0} K_j(t_n + \epsilon)$, $K_j(t_{n+1}^-) = \lim_{\epsilon \downarrow 0} K_j(t_{n+1} - \epsilon)$, and $\mathcal{Q}_j^n = \partial \mathcal{K}_j^n \setminus (K_j(t_n^+) \cup K_j(t_{n+1}^-))$.

We denote with S^n the set of all faces in the space-time slab E^n (see Fig. 3c for an illustration). The set $\mathcal{S}_I^n$ is the set of all internal faces, where each internal face is shared by two elements. At the slab boundary $\mathcal{Q}^n$, we have the set of boundary faces $\mathcal{S}_B^n$. This set is the union of the sets $\mathcal{S}_D^n$ and $\mathcal{S}_M^n$, which are related to the Dirichlet and mixed boundary conditions, respectively.

4 DG FORMULATION

In this section, we summarize the space-time DG method. More details on this method can be found in [8] and [9]. First, we present the space-time DG method for the convection-diffusion equation (1), then we discuss the time DG method for the moving boundary equation (3).

4.1 Space-time DG method for convection-diffusion equation

We consider a tesselation $\mathcal{T}_h$ of space-time elements $\mathcal{K}$. Each element $\mathcal{K}$ is related to the reference element $\hat{\mathcal{K}} = (-1,1)^3$ using an isoparametric mapping $G_j^n : \hat{\mathcal{K}} \to \mathcal{K}_j^n$. The finite element space then is defined as

$$V_h := \{u \in L^2(E) : u|_{\mathcal{K}} \circ G_j^n \in \mathcal{Q}_k(\hat{\mathcal{K}})\}, \tag{4}$$

with $\mathcal{Q}_k(\hat{\mathcal{K}})$ the set of all tensor-product polynomials on $\hat{\mathcal{K}}$ of degree $k \geq 1$ in each coordinate direction. We also introduce an auxiliary finite element space Σ_h, defined as

$$\Sigma_h := \{\tau \in L^2(E)^2 : \tau|_{\mathcal{K}} \circ G_j^n \in \mathcal{Q}_k(\hat{\mathcal{K}})^2\}.$$

Note that the finite element spaces V_h and Σ_h do not impose any continuity across element faces, both in space and time. The unit outward space-time normal vector at the element boundary $\partial \mathcal{K}_j^n$ is denoted with n. This normal vector can be written as $n = (n_0, \bar{n})$, with $n_0 \in \mathbb{R}$ the temporal component of the normal vector and $\bar{n} \in \mathbb{R}^2$ the spatial component of the normal vector. Following the analysis in [10], the temporal component of the normal vector n_0 at the element boundaries $K_j(t_n^+)$ and $K_j(t_{n+1}^-)$ is equal to -1 and 1, respectively, while the spatial component $\bar{n}$ at those element boundaries vanishes. At the faces $S \in \mathcal{Q}_j^n$ the space-time normal vector n is equal to

$$n = (n_0, \bar{n}) = (-\nu \cdot \bar{n}, \bar{n}),$$

with $\nu \in \mathbb{R}^2$ the velocity of the point where the normal vector is evaluated [10, 11].

In order to deal with the discontinuities at the element boundary of functions in V_h and Σ_h, we introduce the average $\{\!\{\cdot\}\!\}$ and jump $[\![\cdot]\!]$ operators on each face S^n. Using the notations $v_i := v|_{\mathcal{K}_i}$, $\tau_i := \tau|_{\mathcal{K}_i}$, and $\bar{n}_i := \bar{n}|_{\mathcal{K}_i}$, the average operator for $\tau \in \Sigma_h$ and the jump operator for $v \in V_h$ are defined as

$$\begin{aligned}
\{\!\{\tau\}\!\} &= (\tau_i + \tau_j)/2, &\quad \text{on } S^n \in \mathcal{S}_I^n, &\qquad [\![v]\!] = v_i \bar{n}_i + v_j \bar{n}_j, &\quad \text{on } S^n \in \mathcal{S}_I^n, \\
\{\!\{\tau\}\!\} &= \tau, &\quad \text{on } S^n \in \mathcal{S}_B^n, &\qquad [\![v]\!] = v\,\bar{n}, &\quad \text{on } S^n \in \mathcal{S}_B^n,
\end{aligned}$$

with $S^n \in \mathcal{S}_I^n$ a face shared by elements $\mathcal{K}_i$ and $\mathcal{K}_j$. We also introduce the local lifting operators r and r_{g_D} [8] as follows

$$\sum_{j=1}^{N_n} \int_{\mathcal{K}_j^n} r(\phi) \cdot q \, d\mathcal{K} = -\int_{S^n} \phi \cdot \{\!\{q\}\!\} dS, \quad \text{on } S^n \in \mathcal{S}_I^n \cup \mathcal{S}_D^n, \tag{5}$$

$$\sum_{j=1}^{N_n} \int_{\mathcal{K}_j^n} r_{g_D}(\phi) \cdot q \, d\mathcal{K} = \sum_{j=1}^{N} \int_{\mathcal{K}_j^n} r(\phi) \cdot q \, d\mathcal{K} + \int_{S^n} g_D \bar{n} \cdot q \, dS, \quad \text{on } S^n \in \mathcal{S}_D^n, \tag{6}$$

for any $\phi, q \in \Sigma_h$. Note that the support of operators r and r_{g_D} for $S^n \in \mathcal{S}_I^n$ is contained in the two elements that share the face S^n.

Denoting with $c_h \in V_h$ an approximation to c, the space-time DG method for the convection-diffusion equation (1) is formulated as follows: Within each space-time slab E^n, find a $c_h \in V_h$ such that the following holds for all $v \in V_h$:

$$\sum_{j=1}^{N_n} \int_{\mathcal{K}_j^n} \left(-\frac{\partial v}{\partial t} c_h + \nabla v \cdot \left(\nabla c_h - u c_h \right) \right) d\mathcal{K}$$

$$+ \sum_{j=1}^{N_n} \int_{K_j(t_{n+1}^-)} v \, c_h dK - \sum_{j=1}^{N_n} \int_{K_j(t_n^+)} v \, c_h^\star dK$$

$$+ \sum_{S^n \in \mathcal{S}_I^n} \int_{S^n} \left(-\{\!\{\nabla v\}\!\} \cdot [\![c_h]\!] + [\![v]\!] \cdot \left(-\{\!\{\nabla c_h\}\!\} - \eta_0 \{\!\{r([\![c_h]\!])\}\!\} + (u - \nu) \, H(c_h^i, c_h^j) \right) \right) dS$$

$$+ \sum_{S^n \in \mathcal{S}_D^n} \int_{S^n} \left(\nabla v \cdot \bar{n}(g_D - c_h) + v\bar{n} \cdot \left(-\nabla c_h - \eta_0 r_{g_D}([\![c]\!]) + (u - \nu) \, H(c_h, g_D) \right) \right) dS$$

$$+ \sum_{S^n \in \mathcal{S}_M^n} \int_{S^n} \left(v(\alpha c_h - g_M) + v\bar{n} \cdot (u - \nu) \, c_h \right) dS = 0. \tag{7}$$

The first term in (7) is the same as when we use a standard Galerkin finite element method. The other terms are added because of the discontinuities in the basis functions across element faces; the terms in the second line are due to discontinuities in time, the terms in the third and fourth line result from the discontinuities in space. The notation $c_h^\star$ refers to the function c_h in the previous space-time slab E^{n-1} evaluated at $K_j(t_n^-)$. The functions c_h^i, c_h^j refer to c_h in the elements $\mathcal{K}_i$ and $\mathcal{K}_j$ evaluated at their common face $S^n \in \mathcal{S}_I^n$. The notation H is used to denote a standard upwind flux. The parameter η_0 is chosen $\eta_0 > 6$ for stability reasons, see [8] for details.

4.2 Time DG method for the moving boundary equation

Let us consider the time interval $\mathcal{I} = (0, T) = \cup_{n=0}^{N_t-1} I_n$ with I_n the nth time interval $I_n = (t_n, t_{n+1})$. We assume that each interval I_n is the image of a reference element $\hat{I} = (-1, 1)$ using a linear mapping F_t. Denoting the position of a point at the boundary as $s(t) = (x, y)^T$, with coordinates x, y at time t, then the movement of the boundary can be written as

$$\frac{ds(t)}{dt} = -\beta^{-1}(\nabla c \cdot \bar{n})\bar{n}. \tag{8}$$

Each component of $s(t)$ in the time interval I_n is approximated with functions in the finite element space Θ_h, which is defined as

$$\Theta_h = \{w \in L^2(\mathcal{I}) : w|_I \circ F_t \in \mathcal{P}_k(\hat{I})\}, \tag{9}$$

with $\mathcal{P}_k$ the set of polynomials of degree $k \geq 1$. The trace of functions $w \in \Theta_h$ at the boundary of the time interval is defined as

$$w(t^{\pm}) = \lim_{\epsilon \to 0} w(t \pm \epsilon).$$

Denoting s_h as an approximation to s in Θ_h, the time DG method for (8) is defined as follows: Within each time interval I_n, find $s_h \in \Theta_h$ such that the following formulation holds for all $w \in \Theta_h$:

$$w(t_{n+1}^-)s_h(t_{n+1}^-) - w(t_n^+)s_h(t_n^-) - \int_{I_n} \frac{dw}{dt} s_h dt = -\beta^{-1} \int_{I_n} w(\nabla c_h^* \cdot \bar{n})\bar{n}dt, \qquad (10)$$

wiht the function $c_h^* \in V_h$ the same as in (7).

5   MESH ADAPTATION

The governing equations (1) and (3) are coupled, which would require that they are solved simultanously. Since this increases the complexity of the simulation, in many references, e.g. [6, 7, 12], these equations are solved decoupled, which results in the following algorithm. In each time step, first the concentration field $c(t_{n+1})$ at time t_{n+1} is calculated by solving the convection-diffusion equation (1) in the domain at $t = t_n$. Then $c(t_{n+1})$ is used in (3) to evaluate the new position of the cavity boundary. After moving the boundary, the value of $c(t_{n+1})$ has to be interpolated to the new position. This can lead to a significant error in the numerical approximation. Especially in the beginning of the etching simulation, when the cavity boundary is flat and moves downwards and under the mask at t_1 (Fig. 4).
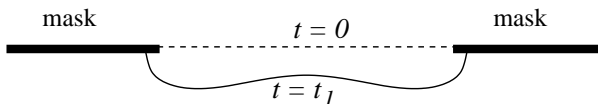

Figure 4: Time evolution of moving boundary in the beginning of etching process.

Using space-time elements, we can avoid this interpolation process. Our algorithm to handle the initial mesh works as follows. At $t = 0$ we divide the boundary on the slit into space elements K_j^0. Even though their coordinates in space at $t = 0$ are the same, these elements relate to different space-time elements (Fig. 5a). We also define an initial mesh at $t = t_1$. This computational domain is divided into elements K_j^1 (Fig. 5b). The space-time elements $\mathcal{K}_j^0$ are constructed by connecting the elements K_j^0 and K_j^1, see Fig. 5c. With this construction we can deal with the degenerated space elements at $t = 0$, since the space-time elements have non-zero volume, and the zero volume of the space elements K_j^0 causes no difficulties in a space-time DG discretization.
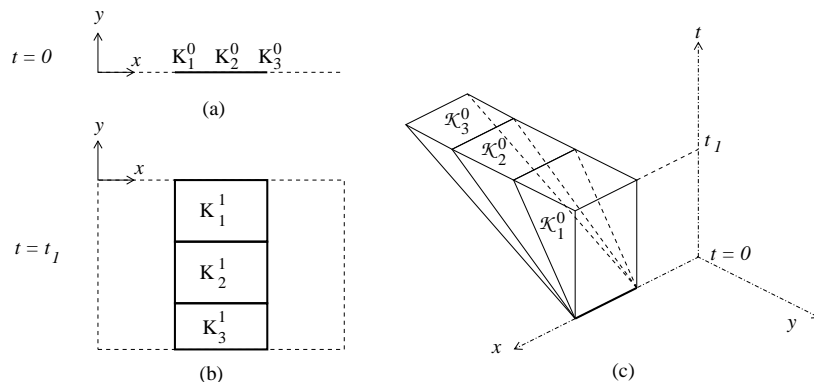
Figure 5: Illustration of the construction of initial elements. (a) Elements at $t = 0$. (b) Elements at $t = t_1$. (c) Construction of space-time elements in I_0.

The actual coordinates of the space elements K_j^1 at $t = t_1$ are obtained by solving the non-linear algebraic equations in the space-time discretization. Since the non-linearity originates from the unknown position of the domain boundary we perform an iteration procedure until convergence is achieved in both the concentration c_h and the boundary position. This process does not require an interpolation of c_h and is fully conservative. We only need to find a reasonable initial guess for the shape of the cavity at the first time level $t = t_1$. One option is to use the solution of the interface position δ of a one-space dimensional mathematical model for an etching process, see [5], as the initial shape of cavity at $t = t_1$ (see Fig. 6):

$$\delta = 2\gamma(D\,t_1)^{1/2},$$

where the value of γ is a known function of the parameter β, see [5]. The iteration procedure will change this shape to the actual (numerical) shape.
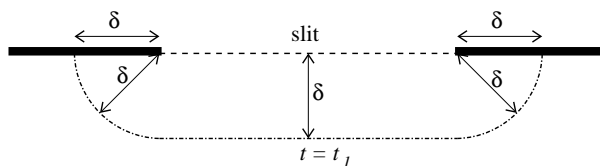

Figure 6: Initial guess of cavity shape at $t = t_1$.

6   NUMERICAL RESULTS

In this section we investigate two model problems: wet-chemical etching of a slit when there is no fluid flow (pure diffusion) and the effect of fluid flow on the etching process (convection-diffusion). The value of the parameter β in (3) for the etching system is

9

typically large [5]. We take a value $\beta = 100$ for all simulations discussed in this paper, which is the smallest value for some typical etching system tabulated in [5]. Here we only present the numerical results for the shape of the cavity during time evolution as this is the primary focus of interest in real applications.

6.1   Pure diffusion wet-chemical etching process

First, we consider the model problem when there is no fluid flow and the diffusion process controls the etching. We assume that the flow domain is already filled with etchant, hence initially the etchant concentration is equal to the inflow concentration. On the far field boundaries $\Gamma_3, \Gamma_4, \Gamma_5$ (see Fig. 2) the concentration is kept equal to the initial concentration. It is assumed that the fluid can not flow through the mask Γ_2. The boundary and initial conditions taken from [12] are:
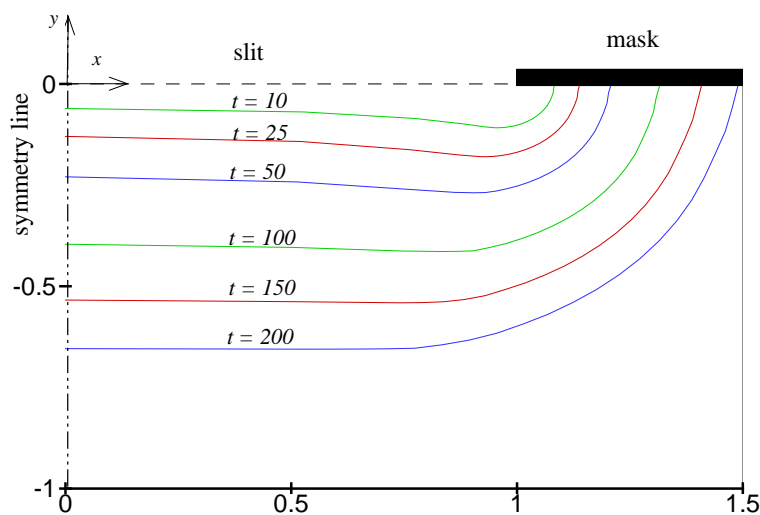

Figure 7: Shape of cavity during time evolution for pure diffusion process. Etching parameters: $S_h = 1000$, $\beta = 100$.

$$
\begin{aligned}
\nabla c \cdot \bar{n} &= -S_h c && \text{on} && \Gamma_1, \\
v_n &= -\beta^{-1} \nabla c \cdot \bar{n} && \text{on} && \Gamma_1, \\
\nabla c \cdot \bar{n} &= 0 && \text{on} && \Gamma_2, \\
c &= 1 && \text{on} && \Gamma_3, \Gamma_4, \Gamma_5, \\
c &= 1 && \text{in} && \Omega \quad \text{at } t = 0.
\end{aligned}
$$

10

First, we choose the Sherwood number $S_h = 1000$ as an example of the etching process when the surface reaction is very fast ($S_h \to \infty$). The shape of the cavity surface resulting from the simulation is shown in Fig. 7.

The figure shows how the shape of the cavity is changing in time. Since the problem is symmetric with respect to the x axis, the figure only shows half of the shape. Because of the fast surface reaction, in the early time of etching process, a bulge is formed near the corner of the mask. Later, when the flow domain under the mask is large enough, this bulge vanishes, i.e. the final shape becomes convex. This phenomenon is described in [4], and confirms our simulation results.
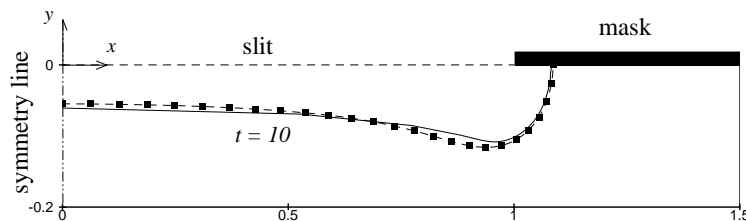

Figure 8: Comparison between numerical results (solid line) and asymptotic solution ($\blacksquare$ symbol) at $T = 10$ with parameter $S_h = 1000$, $\beta = 100$.

For the simulation with fixed far field boundaries $\Gamma_3, \Gamma_4, \Gamma_5$, as used for instance in [12], the boundary condition at these boundaries has to be adapted at large time. An asymptotic approximation of the concentration, derived in [4], is used in [12] to prescribe the far field boundary condition at large time. Using the time-dependent domain, we can avoid the changing of the boundary condition. Instead, we move the position of the far field boundary further away during the simulation to account for the changes in the diffusion field to allow a fixed prescribed concentration at these boundaries. A comparison between the simulation and the asymptotic solution [4] is shown in Fig. 8. The figure shows good agreement between the numerical result and the asymptotic approximation.

Next, we perform a simulation for the Sherwood number $S_h = 1$, which is an example when the surface reaction proceeds slowly compared to the transport of the etchant. Here the kinetics controls the transport process and the concentration is assumed to be the same everywhere. For small values of the Sherwood number, the bulge phenomenon is less pronounced and the moving boundary moves slower than for large values of S_h (see Fig. 9).
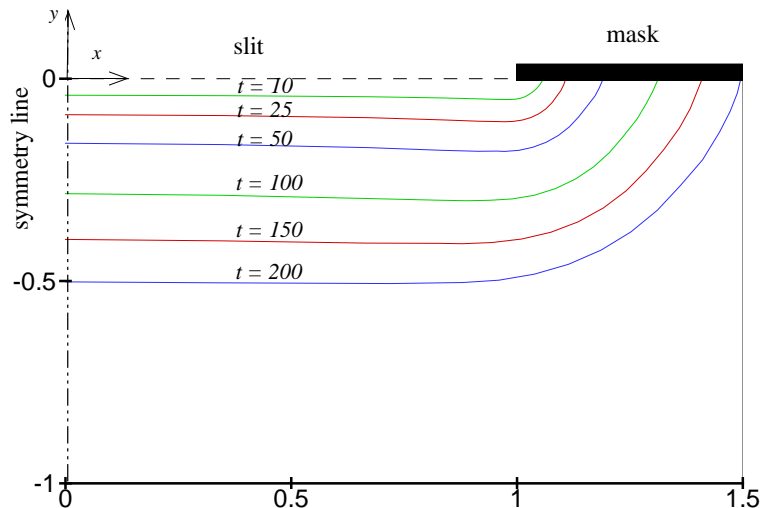
11

Figure 9: Shape of cavity during time evolution for pure diffusion process. Etching parameters: $S_h = 1$, $\beta = 100$.

6.2 Wet chemical etching process with a prescribed fluid velocity field

In this section we consider a model problem when there is fluid flow coming into the domain, see Fig. 10 for a schematic sketch of the flow domain. The boundary and initial conditions for this model are similar to the model in [7]:

$$
\begin{aligned}
\nabla c \cdot \bar{n} &= -S_h c && \text{on} \quad \Gamma_1, \\
v_n &= -\beta^{-1} \nabla c \cdot \bar{n} && \text{on} \quad \Gamma_1, \\
\nabla c \cdot \bar{n} &= 0 && \text{on} \quad \Gamma_2, \Gamma_4, \Gamma_5, \\
c &= 1 && \text{on} \quad \Gamma_3, \\
c &= 1 && \text{in} \quad \Omega \quad \text{at } t = 0.
\end{aligned}
$$

Instead of solving the Navier-Stokes equations for fluid velocity u as in [6], we prescribe the velocity field u with functions that resemble the behaviour of the fluid flow in the domain. First, we assume that the velocity $u = (u_x, u_y)^T$ has a following profile:

$$
\begin{cases}
u_x = \zeta y, & u_y = 0, & y > 0, & \zeta > 0 \\
u_x = 0, & u_y = 0, & y \leq 0,
\end{cases}
\tag{11}
$$

hence we assume that the velocity field only has nonzero values in the region above the mask. We realize that this is a rough approximation, but we will refine this choice later.
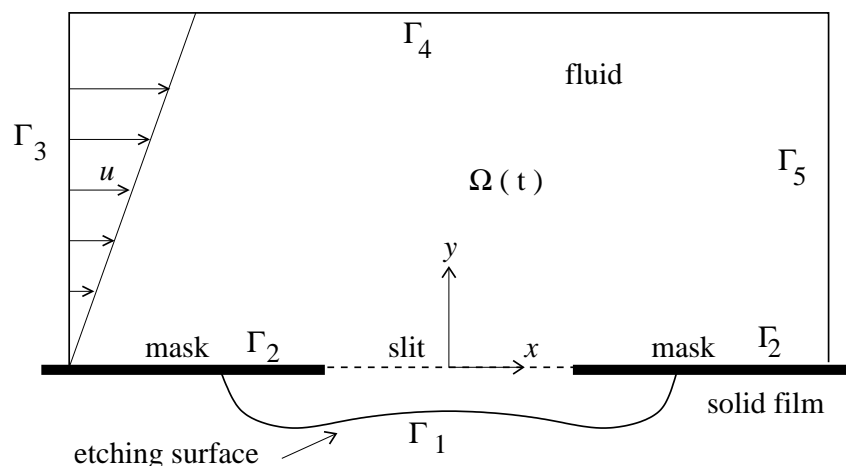
Figure 10: Flow domain of a slit with prescribed flow field u.

Simple scaling arguments show that ζ is propotional to

$$\zeta = P_e \frac{D}{L^2}, \tag{12}$$

with D the diffusion coefficient and L the length scale. In a typical wet-chemical etching process, the diffusion coefficient is of the order 10^{-9} and the length scale of the order 10^{-5}. Hence, we assume that the value of ζ is of the order $10\,P_e$.

We perform the numerical simulation for a Péclet number $P_e = 100$ and a Sherwood number $S_h = 1000$. The resulting shape of the cavity is shown in Fig. 11. We can clearly see the non-symmetric evolution of the shape due to the fluid flow. As the flow comes from the left, the concentration of the etchant is higher on the left side, compared to the right side. Meanwhile, due to the fast reaction at the moving surface, the concentration along this surface is equal to zero. Hence the gradient of the concentration on the left side of the cavity is higher than on the right side and, since the movement of the cavity boundary depends linearly on the magnitude of the gradient of the concentration at the boundary, the boundary on the left side moves(etches) faster than on the right side. For small times this is indeed confirmed by the numerical simulations in, e.g. [3, 6].

For longer times, however, it is known [3] that the non-symmetry becomes of a different character: the right side becomes deeper and our approximation does not capture that. Of course this can be understood physically, because for longer times there is a flow from left to right within the cavity which effectively transports the echant material to the right, and as a consequence starts to speed up the etching process in the right part of the cavity.

In order to adopt this behaviour of the fluid flow, we apply a refined (but still very simple) approximation of the velocity field u. We define the velocity field as being non-zero above the mask, but we now extend thw velocity field into the cavity. This is accomplished by assuming that the streamline at Γ_2 moves down from the left mask edge point A to
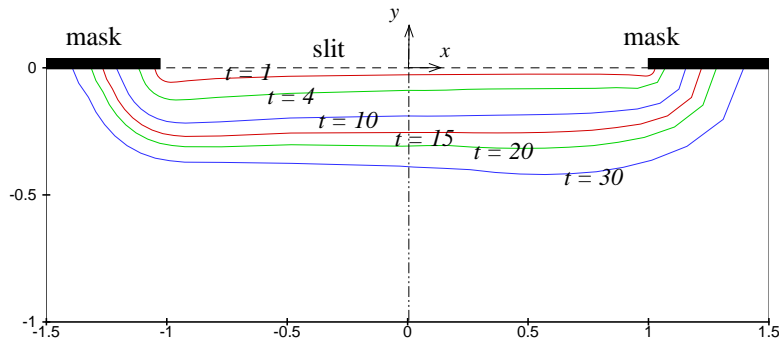
13

Figure 11: Shape of cavity during time evolution. Fluid flows from the left with nonzero velocity u on the region above the mask. Etching parameters: $S_h = 1000$, $\beta = 100$, $P_e = 100$.

the point B at the middle of the cavity boundary and up to right mask edge C (see Fig. 12). We assume that the velocity has a linear profile in the vertical direction and matches the boundary value at Γ_4.
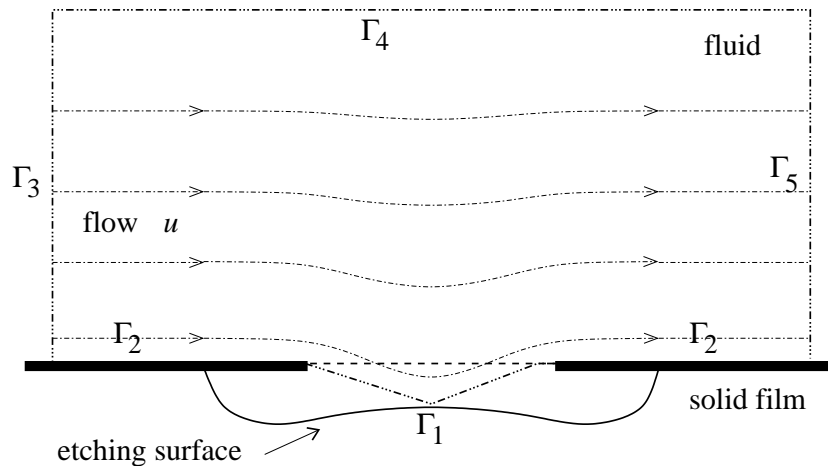

Figure 12: Fluid velocity u profile above the mask and into the cavity.

The result of this simulation is shown in Fig. 13. Qualitatively this behaviour is very good compared to numerical solutions which also involve a full simulation of the Navier-Stokes equations, e.g. [6, 7] (of course we cannot expect quantitive agreement with such models). It does show, however, that the space-time DG method is quite capable of giving reliable results for convection-diffusion problems simulating wet-chemical etching processes, including the effect of transport and fluid flow on the shape evolution of the moving boundary.
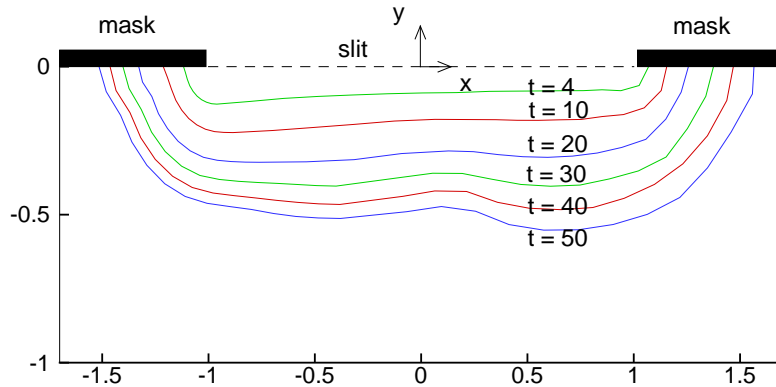
14

Figure 13: Shape of cavity during time evolution. Fluid flows from the left on the region above the mask and into the cavity. Etching parameters: $S_h = 1000$, $\beta = 100$, $P_e = 100$.

7 CONCLUSIONS

In this paper we showed applications of the space-time discontinuous Galerkin method to simulations of wet-chemical etching. The DG method has a local discretization and is easily combined with hp adaptation, which is needed for this application, since we have to deal with irregular meshes, solid-etchant interface, and incompatible initial data.

Inclusion of the time variable into the complete discrezation is beneficial as we have to deal with time-dependent domains. In this way, we have no difficulties with deforming and even degenerated spatial elements. An additional benefit of the space-time DG discretization in wet-chemical etching is related to the generation of the initial shape of the cavity at the start of the etching process. Using a simple but reasonable initial shape, an accurate numerical shape is obtained after several iterations and a complicated interpolation procedure can be avoided. The DG method has, however, some disadvantages compared to a standard/continuous Galerkin discretization. The formulation of the DG method is more complex than for a continuous elements and more integrations on the element boundaries are needed.

The space-time DG method is applied to different etching problems, where either the diffusion or the convection dominates the process. When the etching process is diffusion-controlled, the numerical shape of the cavity resulting from the space-time DG method give good agreement with analytical studies. We also find the typical asymmetric etching cavities for convection-dominated processes, even though we only use a simple model for the fluid velocity field, instead of solving the full Navier-Stokes equations. In order obtain also a good quantitative agreement for convection-dominated wet-chemical etching processes, we have to include the Navier-Stokes equations for the fluid flow into the mathematical model, which is presently being carrried out.

15

ACKNOWLEDGEMENT

REFERENCES

[1] D.N. Arnold, F. Brezzi, B. Cockburn, and L.D. Marini. Unified analysis of discontinuous Galerkin methods for elliptic problems. *SIAM J. Numer. Anal.*, **39** (5), 1749–1779, 2002.

[2] B. Cockburn and C.W. Shu. Runge-Kutta discontinuous Galerkin method for convection-dominated problems. *J. Sci. Comput.*, **6** (3), 173–261, 2001.

[3] C.H. Driesen, *Simulation of Convection-Driven Wet-Chemical Etching*, PhD Thesis, University of Twente, 1999.

[4] H.K. Kuiken. Etching through a slit. *Proc. R. Soc. Lond. A*, **396**, 95–117, 1984.

[5] H.K. Kuiken, J.J. Kelly, and P.H.L. Notten. Etching profiles at resist edges. Part I. Mathematical models for diffusion-controlled cases. *J. Electrochem. Soc.*, **133** (6), 1217–1226, 1986.

[6] C.B. Shin and D.J. Economou. Effect of transport and reaction on the shape evolution of cavities during wet chemical etching. *J. Electrochem. Soc.*, **136** (7), 1997–2004, 1989.

[7] C.B. Shin and D.J. Economou. Forced and natural convection effects on the shape evolution of cavities during wet chemical etching. *J. Electrochem. Soc.*, **138** (2), 527–538, 1991.

[8] J.J. Sudirham, J.J.W. van der Vegt, and R.M.J. van Damme. *Space-time discontinuous Galerkin method for parabolic problems in time-dependent domain.* Memorandum Department of Applied Mathematics, University of Twente, The Netherlands, 2004.

[9] J.J. Sudirham, J.J.W. van der Vegt, and R.M.J. van Damme. Space-time discontinuous Galerkin method for convection-diffusion problems with moving boundaries: application to wet-chemical etching, submitted to *Applied Numerical Mathematics*, 2004.

[10] J.J.W. van der Vegt and H. van der Ven. Space-time discontinuous Galerkin finite element method with dynamic grid motion for inviscid compressible flows, Part I. general formulation. *J. Comput. Phys.*, **182** (2), 546–585, 2002.

[11] H. van der Ven and J.J.W. van der Vegt. Space-time discontinuous Galerkin finite element method with dynamic grid motion for inviscid compressible flows, Part II. Efficient flux quadrature. *Comput. Methods Appl. Mech. Engrg.*, **191** (41-42), 4747–4780, 2002.

[12] C. Vuik and C. Cuvelier. Numerical solution of an etching problem. *J. Comput. Phys.*, **59**, 247–263, 1985.